ARCTIC MIXED-PHASED CLOUD MICROPHYSICAL PROPERTIES RETRIEVED FROM GROUND-BASED ACTIVE AND PASSIVE REMOTE SENSORS

Zhien Wang[1,3], Kenneth Sassen[2], David Whiteman[3], and Belay Demoz[3]

[1]GEST Center, University of Maryland, Baltimore County, E-mail: zhien@agnes.gsfc.nasa.gov

[2]University of Alaska, Fairbanks, Alaska 99775,

[3]NASA Goddard Space Flight Center, Greenbelt, MD 20771

1. INTRODUCTION

The impact of a cloud system strongly depends on the cloud microphysical properties and its vertical extent (Stephens et al. 1990; Baker 1997). Although clouds can contain only water droplets when > 0°C and only ice crystals when < −40 °C, between 0 and −40 °C, clouds can be of ice, water, or mixed-phase composition (Rauber and Tokay 1991; Cober et al. 2001). Among them, mixed-phase clouds are poorly understood. However, properly representing them in general circulation models (GCMs) is very important for climate simulations (Fowler et al.,1996; Li and Le Treut 1992; Sun and Shine 1994; Gregory and Morris 1996). The internal structures of mixed-phase clouds have large variations among different cloud types and latitudes. In low- and mid-latitude, mixed-phase clouds are often associated with convective clouds, on the other hand, mixed-phase clouds usually exist in stratiform in the Polar region.

The results of the Surface Heat Budget of the Arctic (SHEBA) experiment indicate that most of Arctic boundary layer clouds are mixed-phase clouds (Shupe et al.,2001; Intrieri et al. 2002). Therefore, mixed-phase clouds play a particularly important role in the Arctic climate system. Curry et al. (1996) gave a comprehensive review of arctic clouds and their role in the Arctic climate system, and clearly indicated that clouds are important to better understand arctic cloud-radiation-surface-dynamics feedbacks. The recent study of Vavrus (2004) indicated that cloud-feed back contribute significantly to the Arctic worming. To better predicate climate change in the Arctic, we need to better understand mixed-phase cloud and to improve it representation in GCMs.

Mixed-phase cloud microphysical properties have been mainly studied with in situ measurements (Fleishauer et al. 2002; Hogan et al. 2003; Korolev et al. 2003), which provide detailed microphysical properties to understand the physical processes controlling mixed-phase clouds. To better understand mixed-phase clouds in different climate regions over a long period, we

have to explore the capability of remote sensing. Radar-only based remote sensing algorithms of mixed-phase clouds (Sauvageot 1996; Vivekanandan et al. 1999; Shupe et al. 2004) are not practical for many stratiform mixed-phase clouds, especially in the Polar region. Based on The Department of Energy Atmospheric Radiation Measurement (ARM) program Cloud and Radiation Testbed (CART) sites observations, we developed a new algorithm to retrieve the microphysical properties of supercooled water with ice virga, a major type of mixed-phase cloud the Arctic, by combining active and passive remote sensor measurements (Wang et al. 2004).

To better characterize arctic mixed-phase cloud, we are applying the algorithm to the longtime multi-sensor observations at the North Slope of Alaska (NSA) CART site. This paper presents two case studies and initial statistical results of mixed-phase cloud microphysical and macrophysical properties at the NSA site.

2. OBSERVATIONS

The observations used in this study are from two active sensors: Millimeter-wavelength cloud radar (MMCR) and Micropulse lidar (MPL), and two passive sensors: Microwave radiometer (MWR) and atmospheric emitted radiance interferometer (AERI). The MMCR is a zenith-pointing radar with a 2-m diameter antenna that operates at 34.86 GHz (8.7-mm wavelength); it has a sensitivity of about -50 dBZ at 5.0 km altitude. This powerful Doppler radar, working in cycles of four sequential modes with selectable parameters, can detect most of the clouds in the troposphere from stratus to cirrus. The MPL is a compact eye-safe lidar that measures cloud base heights and aerosol profiles from the surface to about 20 km in the absence of strongly attenuating clouds. Eye-safety allows for full-time, long-term unattended operation, and is achieved by transmitting low power pulses through an expanded beam, with a much higher pulse repetition frequency than that used in standard lidar systems. The MMCR can penetrate optically thick clouds to detect multi-layer cloud systems.

However, its long wavelength limits its capability to detect midlevel supercooled water clouds with relatively small water droplets. For mixed-phase clouds or water clouds with drizzle, MMCR signals are dominated by the backscatter of ice particles or drizzle-size droplets. MPL are senstive enough to detect all clouds in the troposphere expect for thin cirrus during day time. The main limitation for MPL and other ground-based lidar is that the strong attenuation of clouds limits lidar capability to detect upper cloud layer in the presence of low-level optically thick cloud layer. Combining MMCR and MPL provide up better capability for cloud detection (Wang and Sassen 2001).

The MWR receives nadir microwave radiation from the sky at 23.8 GHz and 31.4 GHz. Path integrated water vapor and liquid water can be retrieved from MWR measurements. Statistical retrieval methods are usually employed to derive water vapor path and liquid water path (LWP) from the total absorption. In current ARM data, the regression residual error or 'theoretical accuracy' of LWP is about 0.03 mm (30 g/m^2) or 10 times the sensitivity or noise limit (0.003 mm) of the MWR. This detectable level limits MWR capability to measure the LWP of many supercooled clouds and mixed-phase clouds.

The "heart" of the AERI radiometer is a Fourier-transform infrared (IR) spectrometer, including the calibration blackbodies with temperature controllers. The AERI measures the absolute infrared spectral radiance of the sky also in the nadir direction. The spectral measurement range of the instrument is 500 to 3300 cm^{-1} (20 to 3 µm) with a spectral resolution of 1.0 cm^{-1}. In our algorithm, we use AERI measurements to retrieve water dominated source cloud property. Compared with the MWR, AERI based retrieval covers the low LWP case. Therefore, Combining MWR and AERI measurements, we are able to cover the full spectrum of LWP observed in the Arctic.

The NSA CART observations start from May 1998. But observations with all above instrumnets are not available until January 1999. We are analysing observations from January 1999 to the end of 2003.

3. SUMMARY OF THE ALGORITHM

Supercooled water with ice virga can be generally regarded as two connected cloud layers where the top is the water-dominated source cloud and the bottom is an ice cloud, although it is also necessary to study ice within the water-dominated source cloud. First, we treat ice virga as an independent ice cloud, and apply an existing lidar-radar algorithm to retrieve ice water content (IWC) and general effective size (D$_{ge}$) profiles (Wang and Sassen 2002). Then a new iterative approach is used to retrieve supercooled water cloud properties (LWP and effective radius r$_{eff}$) by minimizing the difference between atmospheric emitted radiance interferometer (AERI) observed radiances and radiances calculated using the discrete ordinate radiative transfer model at 12 selected wavelengths. The flowchart of the algorithm is given in Figure 1, and more information about the algorithm can be found from Wang et al. (2004). Case studies demonstrated the capabilities of this approach in retrieving radiatively important microphysical properties to characterize this type of mixed-phase cloud. The good agreement between visible optical depths derived from lidar measurement and those estimated from retrieved liquid water path and effective radius provided a closure test for the accuracy of mainly AERI-based supercooled water cloud retrieval.
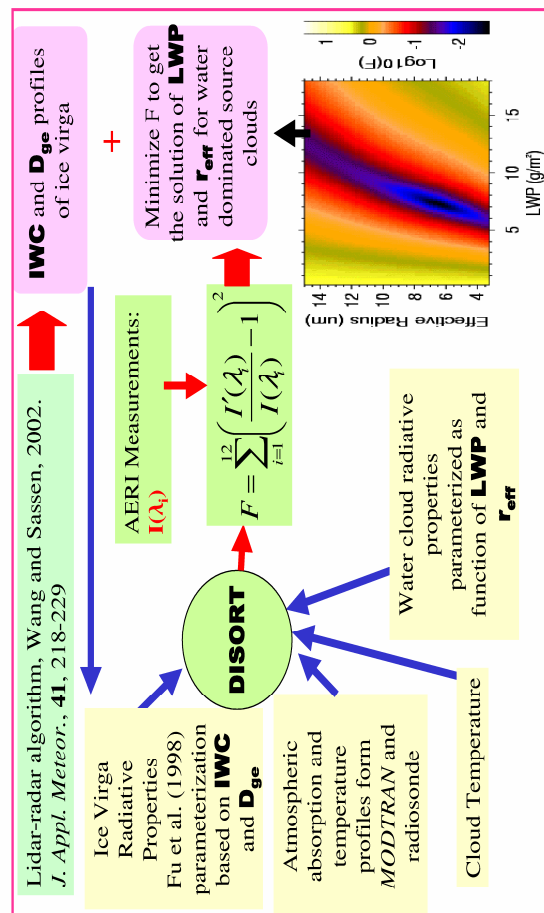

Figure 1. The flowchart of the algorithm

4. CASE STUDIES

The algorithm is applied to the data from the NSA CART site. To show the algorithm capability, we briefly discussed two cases in this section. The first case is a boundary-layer supercooled stratocumulus with ice precipitation. Figure 2 shows radiosonde temperature and relative humidity (RH) profiles obtained at the NSA site at 2259 UTC 1 November 2001. This cloud system lasted more than 30 hours, and the 24-hour observations of MMCR and MPL and retrieved ice and water properties are presented in Fig. 3. The supercooled stratocumulus clouds are clearly indicated by narrow bright band in the time-height display of MPL extinction (Fig. 3b). The ice precipitation is more clearly displayed by Ze profiles in Fig. 3a. The cloud top increased slowly from ~1.5 to ~2.4 km during the 24-hour period. Cloud top temperature was about -26 °C at 2259 UTC, and there was ~4 °C temperature inversion above the cloud top. The RH profile shows relative moisture environments above and below the supercooled water-dominated generating layer. This may be an important factor for the maintenance of this type mixed-phase clouds.
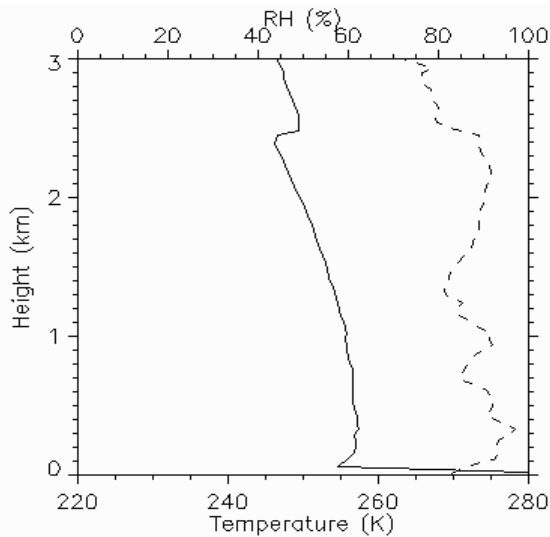
Figure 2. Radiosonde temperature (solid line) and relative humidity (dashed line) profiles obtained at the NSA site at 2259 UTC 1 November 2001.

The retrieved IWC and D_{ge} profiles of ice precipitation are given in Fig. 3c and d. The IWC values range from a few mg/m^3 to ~ 100 mg/m^3, and are usually increase when height decrease

because the boundary layer was ice saturated. The D_{ge} of ice precipitation were between 60 and 160 um. The LWP and r_{eff} of the supercooled water-dominated generating layer are given in the Fig. 3e. The algorithm only can be applied to water cloud with LWP smaller than some values depending somewhat on particle size (Wang et al. 2004). The largest LWP in the retrieval is set at 45 g/m^2, and we use MWR measurements when LWP is larger than this value. Figure 3e shows a large variation of LWP while r_{eff} values are mainly around 5 um.
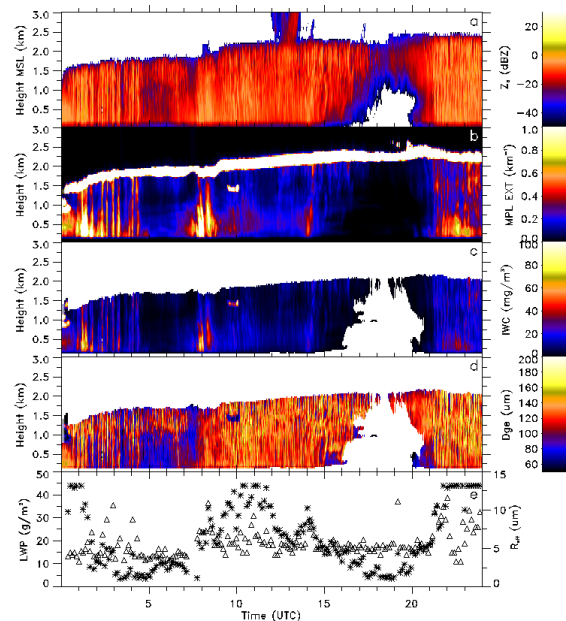
Figure 3. Time-height display of radar reflectivity factor (Ze, a), visible extinction coefficient retrieved from MPL measurements (b), the retrieved IWC (c) and Dge (d) profiles, and supercooled water cloud properties for a stratocumulus cloud with ice precipitation observed at the NSA CART site on 1 November 2001.

The second case is an interesting altocumulus with ice virga observed at the NSA CART site on 2 January 2002, which transited to all ice altostratus in a short period. Figure 4 shows radiosonde temperature and relative humidity (RH) profiles obtained at the NSA site at 2259 UTC 2 January 2002. The time-height displays of MMCR and MPL measurements and retrievals of cloud microphysical properties are presented in Fig. 5a-e. The supercooled water existed until ~ 12 UTC at ~5.5 km height. There was no radiosonde data available during the supercooled water cloud

occurrence; however, radiosonde data at 2259 UTC indicates -30 °C at the supercooled water cloud height.
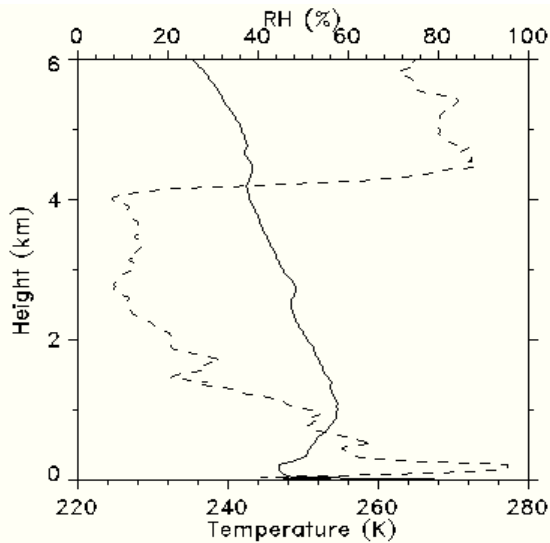
Figure 4. Radiosonde temperature (solid line) and relative humidity (dashed line) profiles obtained at the NSA site at 2259 UTC 2 January 2002.
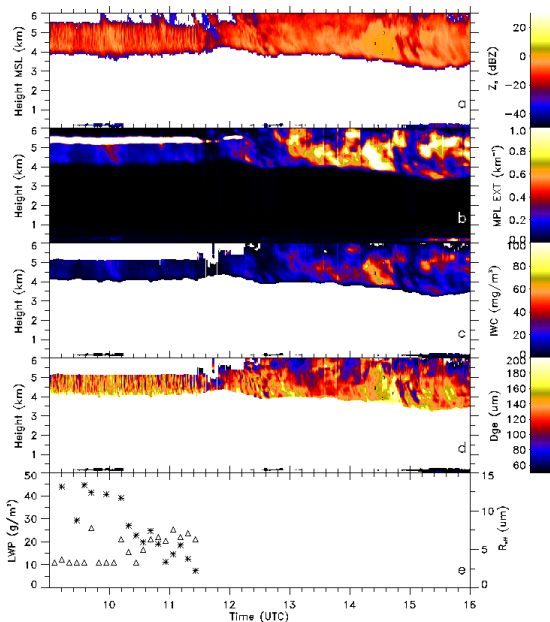

Figure 5. The same as Fig. 3 except for an altocumulus with ice virga on 2 January 2002.

The transition of mixed-phase clouds to all ice clouds happened within an hour as indicated in

Fig. 5b. The IWC values of mixed-phase cloud are smaller than those during all ice period on average. However, the particle sizes of ice virga are similar to those at the same height during all ice period. This suggests that ice particle number concentration in the ice virga is smaller than that in all ice clouds. Understanding the factors maintaining the supercooled water clouds and controlling the transition in this case may be important to better understand cloud physics and dynamics in general, nevertheless, we lack the other necessary information to further explore it.

5. CLOUD MACROPHYSICAL PROPERTIES OBSERVED AT THE NSA CART SITE
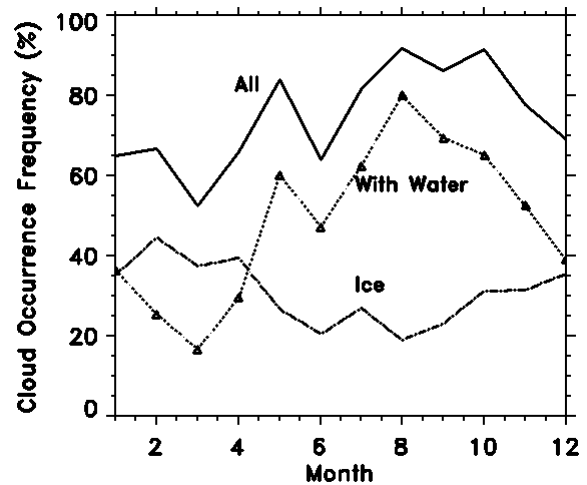
Figure 6. The occurrence frequency of clouds observed by MPL at the NSA CART site from January 2000 to August 2003.

A lidar cloud detection algorithm (Wang and Sassen 2001) is applied to MPL data observed at the NSA CART site. The algorithm is able to identify water cloud base in the presence of virga. For non-precipitating water clouds, it can be easily be distinguished from ice clouds by only using lidar backscattering intensity because water clouds usually have higher extinction or attenuation than ice clouds, though other measurements, such as lidar linear depolarization ratio, are better suited for water and ice cloud discrimination (Sassen 1991). Figure 6 presents cloud occurrences of all clouds, ice clouds, and containing water (including water and mixed-phase clouds). The cloud occurrence at the NSA CART site is high and this is consistent with observations at other locations in the Arctic (Curry et al. 1996). However, the data at the NSA CART site shows a large year to year variation of cloud cover. Cloud layers contained water occurred

~16% in March, but as high as ~80 % in August. A part of these clouds is mixed-phase. We are working to combine MPL and MMCR measurements to better identify mixed-phase cloud.
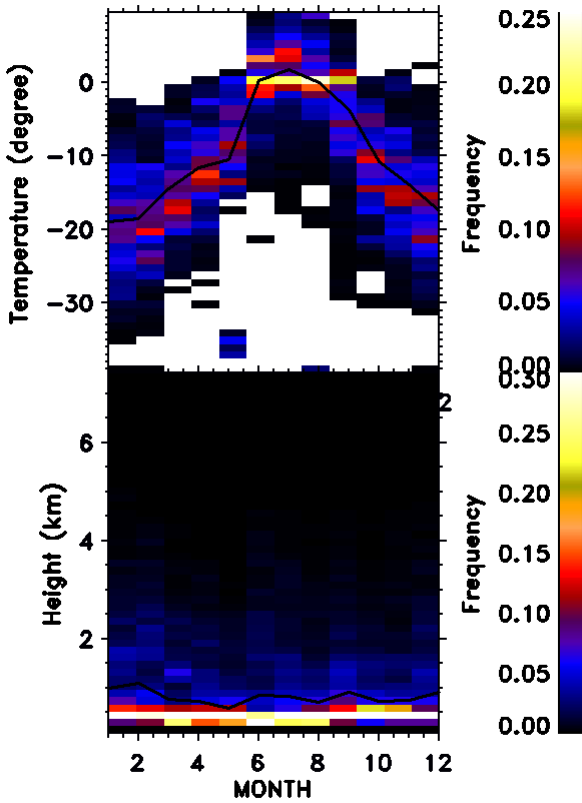

Figure 7. The distributions of cloud base temperature and height observed at the NSA CART site.

The frequency distributions of water layer base (including both mixed-phase and pure water clouds) temperature and height for each month are given the Fig. 7. There is no surprise that there is a strong annual variation of the base temperature. During January, the mean base temperature reaches ~ -19 °C. Except June, July, August, and September, over 95% water layers are supercooled. The water base height mainly locates in the boundary layer. The mean base height ranges from ~ 500 m to ~1000 m.

6. THE STATISTICAL RESULTS OF THE MICROPHYSICAL PROPERTIES OF SUPERCOOLED ALTOCUMULUS WITH ICE VIRGA

The statistical results of microphysical properties of altocumulus with ice virga based on 30 different cases are presented in Figs. 8 and 9. Figure 8 shows the frequency distributions of LWP, r_{eff}, and visible optical depths for ice virga and water. These results indicate a large variation of microphysical properties of this type of mixed-phase clouds. Compared with boundary-level water, the LWP of midlevel cloud is small, and it is also true for r_{eff}. The optical depth of ice virga is much smaller than that of water in this type of mixed-phase clouds in general, but it shows a large variation at different stages of cloud lifecycle as revealed in the case studies.

The statistical results of LWP retrieved from MWR measurements for same cases are presented in Fig. 8 for comparison. It is clear that MWR measurements for low LWP values are not reliable, and the retrieval using the AERI or other IR radiometer measurements provides a good alternative for the low LWP measurements.
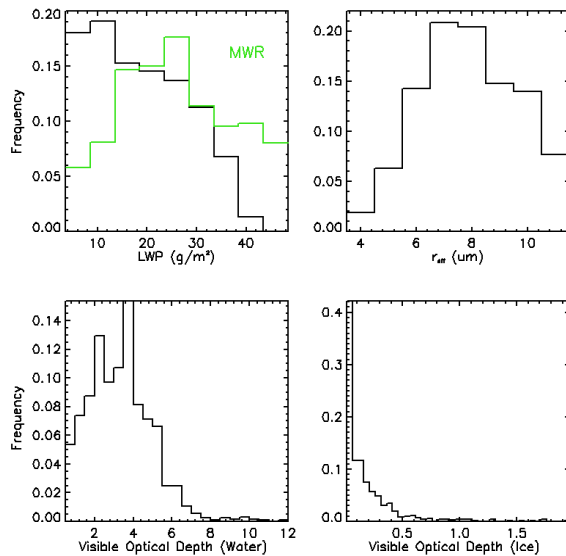
Figure 8. Frequency distributions of LWP, r_{eff}, and the optical depth of supercooled water and ice virga. The frequency distribution of LWP derived from MWR during the same period is plotted in green color.

The temperature dependencies of LWP and r_{eff} are presented in Fig. 9. Both of them increase

with the increase of cloud temperature. The standard deviations of them are given with vertical lines, which indicate large variations of them at given temperatures because many other parameters also control cloud microphysical properties. In the mixed-phase clouds as we studied here, the competition between ice and water phases makes the situation more complicated.
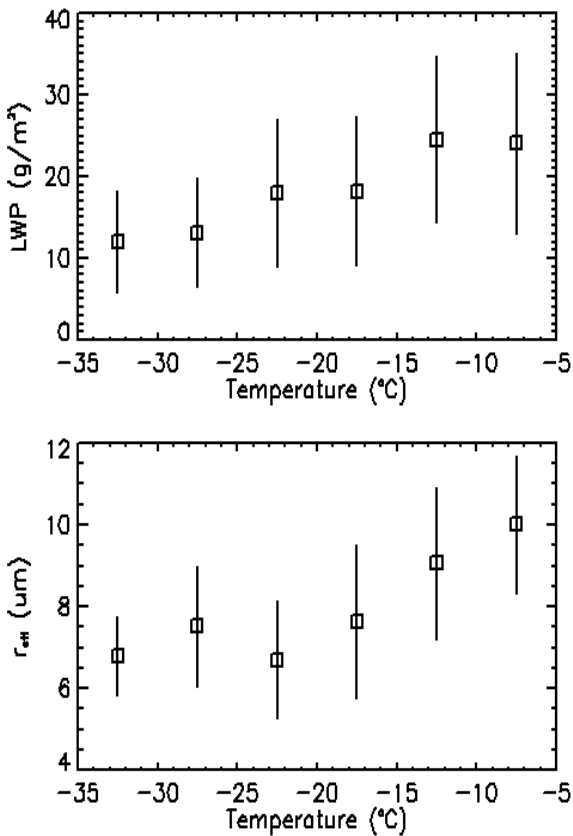
Figure 9. The temperature dependency of LWP and r_{eff}. Vertical lines represent standard deviations.

7. SUMMARY

Based on MPL measurements, the cloud occurrence at the NSA CART site is as high as 90% during the Arctic summer season. Except January to April, more than 50% of cloud layer include water layer. The statistical results of water layer base height and temperature indicate a high occurrence of supercooled water clouds in the Arctic. In the Arctic, the supercooled water layer usually exists with an ice virga layer or ice precipitations to from a simple type mixed-phase cloud. A better characterization of this type mixed-

phase cloud is important to better understand the role of cloud in the arctic climate system.

An approach of combining lidar, radar and radiometer measurements to retrieve the microphysical properties of this type mixed-phase clouds was developed. The approach can retrieve the microphysical properties of water and ice in the cloud layer, which are necessary to better understand cloud microphysical processes in this type of mixed-phase cloud. The retrieval accuracy of LWP and r_{eff} for water-dominated generating layer is ~15%.

The two case studies illustrated the capability of the algorithm for characterizing this type mixed-phase clouds. The initial statistics of microphysical properties of this type of middle-level mixed-phase clouds based on 30 cases is presented. There are apparent temperature dependences for both LWP and r_{eff} of the water-dominated source clouds. Comparison of the retrieved LWP with that retrieved from MWR indicated that MWR is unable to provide reliable low LWP measurements for supercooled altocumulus with ice virga. The mean biases of MWR retrieved LWP can up to 20 g/m^2, which is significant in terms of resulting radiative impacts.

The results presented here are preliminary. The analysis of long-term NSA CART observations is still in progress. Combining retrieved microphysical properties with other observations and model simulations, we are aiming at better understanding the generation, maintenance, and impact of this type mixed-phase cloud in the Arctic.

References
Baker, M. B., 1997: Cloud microphysics and climate, *Science,* **276**, 1072-1078.
Cober, S. G., G. A. Isaac, A. V. Korolev, and J. W. Strapp, 2001: Assessing cloud phase condition conditions, *J. Appl. Meteor.*, **40**, 1967-1983.
Curry, J. A., W. B. Rossow, D. Randall, and J. L. Schramm, 1996: Overview of Arctic cloud and radiation characteristics. *J. Climate*, 9, 1731-1764.
Fleishauer, R. P., V. E. Larson, and T. H. Vonder Haar, 2002: Observed microphysical structure of midlevel, mixed-phase clouds. *J. Atmos. Sci.*, **59**, 1779-1804.

Fowler, L. D., D. A. Randall, and S. A. Rutledge,1996: Liquid and ice cloud microphysics in the CSU general circulation model. Part I: model description and simulated microphysical processes. *J. Climate*, **9**, 489-529.

Gregory, D. and D. Morris, 1996: The sensitivity of climate simulation to the specification of mixed phase clouds. *Climate Dyn.,* 12, 641-651.

Hogan, R., P. Francis, H. Flentje, A. J. Illingworth, M. Quate, and J. Pelon, 2002: Characteristics of mixed-phase clouds part I: lidar, radr and aircraft observations from CLARE'98. *Q. J. R. Meteorol. Soc.*, **129**, 2089-2116.

Hogan, R., A. J. Illingworth, E. J., O'Connor, J. P. V. P. Baptista, 2003: Characteristics of mixed-phase clouds part I: A climatology from ground-based lidar. *Q. J. R. Meteorol. Soc.*, **129**, 2117-2134.

Intrieri, J. M., M. D. Shupe, T. Uttal, and B. J. McCarty, 2002: An annual cycle of Arctic cloud characteristics observed by radar and lidar at SHEBA. *J. Geopys. Res.*, **107**, 8030, doi:10.1029/2000JC000423.

Korolev, A. V., G. A. Isaac, S. G. Cober, J. W. Strapp, and J. Hallett, 2003: Microphysical characterization of mixed-phased clouds. *Q. J. R. Meteorol, Soc.*, **129**, 39-65.

Li, Z.-X., and H. Le Treut, 1992: Cloud-radiation feedbacks in a general circulation model and their dependence on cloud modeling assumptions. *Climate Dyn.*, 7, 133-139

Rauber, R. M., and A. Tokay, 1991: An explanation for the existence of supercooled water at the tops of cold clouds. *J. Atmos. Sci.*, **48**, 1005-1023.

Sassen, K. 1991: The polarization lidar technique for cloud research: A review and current assessment. Bull*. Am. Meteor. Soc.*, **72**, 1848-1866.

Sauvageot, H., 1996: Retrieval of vertical profiles of liquid water and ice content in mixed clouds from Doppler radar and microwave radiometer measurements. *J. Appl. Meteor.*, **35**, 14-23.

Shupe, M. D., T. Uttal, S. Y. matrosov, A. S. Frisch, 2001: Cloud water contents and hydrometer sizes during the FIRE-Arctic cloud experiment. *J. Geopys. Res.*, **106**, 15,015-15,028.

Shupe, M. D., J. M. Intrieri, 2003: Cloud radiative forcing of the Arctic surface: The influence of cloud properties, surface albedo, and solar zenith angle. *J. Climate*, **17**, 616-628

Stephens, G. L., S. Tsay, P. W. Stackhouse, and P. J. Flatau, 1990: The relevance of the microphysical and radiative properties of cirrus clouds to climate and climatic feedback. *J. Atmos. Sci.*, **47**, 1742-1753.

Sun, Z., and K. P. Shine, 1994: Studies of the radiative properties of ice and mixed-phase clouds. *Quart. J. Roy. Meteor, Soc.*, **120**, 111-137.

Vavrus, S., 2004: The impact of cloud feedbacks on Arctic climate under greenhouse forcing. *J. Climate*, **17**, 603-615.

Vivekanandan, J., B. E. Martner, M. K. Politovich, and G. Zhang, 1999: Retrieval of atmospheric liquid and ice characteristics using dual-wavelength radar observations. *IEEE Trans. Geosci. Remote Sensing*, **37**, 2325-2334.

Wang, Z., and K. Sassen, 2001: Cloud type and macrophysical property retrieval using multiple remote sensors. *J. Appl. Meteor.,* **40**, 1665-1682.

Wang, Z. and K. Sassen, 2002: Cirrus cloud microphysical property retrieval using lidar and radar measurements: I algorithm description and comparison with in situ data. *J. Appl. Meteor.*, **41**, 218-229.

Wang, Z., K. Sassen, D. Whiteman, and B. Demoz 2004: Studying altocumulus plus virga with ground-based active and passive remote sensors. *J. Appl. Meteor.,***43**, 449-460.